Electronic Supplementary Material (ESI) for Organic Chemistry Frontiers.

Supplementary information

The effect of a highly twisted C=C double bond on the electronic structures of 9,9'-bifluorenylidene derivatives in the ground and excited states

Atsuro Takai,*[a] Dylan J. Freas,[a] Toshikane Suzuki,[a,b] Manabu Sugimoto,[c] Jan Labuta,[d]
Rie Haruki,[e] Reiji Kumai,[e] Shin-ichi Adachi,[e] Hayato Sakai,[f] Taku Hasobe,[f]
Yoshitaka Matsushita[a] and Masayuki Takeuchi*[ab]

[a] Molecular Design and Function Group, National Institute for Materials Science (NIMS), 1-2-1 Sengen, Tsukuba, Ibaraki 305-0047, Japan.

[b] Department of Materials Science and Engineering, Graduate School of Pure and Applied Sciences, University of Tsukuba, 1-1-1 Tennodai, Tsukuba, Ibaraki 305-8577, Japan

[c] Faculty of Advanced Science and Technology, Kumamoto University, 2-39-1 Kurokami, Chuo-ku, Kumamoto 860-8555, Japan

[d] International Center for Materials Nanoarchitectonics (MANA), National Institute for Materials Science (NIMS), 1-1 Namiki, Tsukuba, Ibaraki 305-0047, Japan

[e] Photon Factory, Institute of Materials Structure Science, High Energy Accelerator Research Organization (KEK), Tsukuba 305-0801, Japan

[f] Department of Chemistry, Faculty of Science and Technology, Keio University, 3-14-1 Hiyoshi, Yokohama, Kanagawa 223-8522, Japan

Table of contents

1. Experimental section

General procedure. Target compounds were purified by a recycling preparative HPLC (LC-9201, Japan Analytical Industry) equipped with gel permeation chromatography columns (JAIGEL-1H + 2H). NMR spectra were recorded on a JEOL ECS-400 spectrometer. Chemical shifts are expressed in ppm relative to $CHCl_3$ (7.26 ppm) and tetramethylsilane (0 ppm) for ^1H NMR and $CDCl_3$ (77.16 ppm) for ^{13}C NMR.[1] ESR spectra were measured on a JEOL X-band spectrometer (JES-FA100) in 1,2-dichlorobenzene using ESR tubes ($\phi = 2$ mm). The sample solutions for both variable-temperature NMR and ESR measurements (25–150 °C) were deaerated by three consecutive freeze-pump-thaw cycles prior to the measurements. MALDI/TOF-MS measurements were performed on a Shimadzu AXIMA-CFR Plus. Absorption and photoluminescence spectra were recorded on a JASCO V-670 spectrophotometer and a PerkinElmer LS-55 spectrofluorophotometer, respectively. Nanosecond laser flash photolysis was carried out with an Unisoku TSP-2000 flash spectrometer. A Surelite-I Nd-YAG (Continuum, 4–6 ns FWHM) laser with the third harmonic at 355 nm was employed for the flash photoirradiation exposure with a xenon lamp (150 W) as probe light and a photomultiplier tube (Hamamatsu R-2949) as detector. Each sample in toluene was purged with Ar prior to the measurement at 25 °C.

Electronic-structure calculation. Computational analysis and graphical representation were carried out with Gaussian 09, revision D.01 and Gauss View software program (version 5), respectively.[2] Molecular orbitals of the single crystal Optimized structures were obtained by M06-2X functional with the 6-31G(d,p) basis set. We also applied the B3LYP and ωB97XD functionals to see the functional dependence of the numerical results, and confirmed that the results are essentially similar. The lower 10 excited states of the compound were studied using time-dependent DFT (TDDFT) method with the same DFT functional and the basis set.

Single crystal X-ray diffraction analysis. A single crystal of **1** was attained by recrystallization from $CHCl_3$ with vapor diffusion of MeOH. All measurements were carried out using a Rigaku AFC11 Saturn724+ diffractometer under 1 atm at 213 K with Mo K_α radiation ($\lambda = 0.71073$ Å). Cell refinement and data reduction were carried out by using the program d*trek package in CrystalClear software suite.[3] Preliminary structures were solved using SHELXT[4] and refined by full-matrix least squares on F^2 using the SHELXL-2016[5] in WinGX program package.[6] All non-hydrogen atoms were refined anisotropically. An alert (level B) of low bond precision on C–C bonds is found in checkCIF report (http://checkcif.iucr.org/), which results from the low crystallinity of **1** probably because of the *cis–trans* equilibrium and severely shadowed diffraction points of **1** by the beam stopper.

Pressure dependent single crystal X-ray diffraction analysis. High pressure was generated using a diamond anvil cell (DAC) with a stainless steel gasket and 0.8 mm culet diamond anvils. The thickness of the gasket was 0.4 mm and the aperture was 90°. Pressure was determined by a conventional ruby-fluorescence method. The DAC was pressurized using a MeOH–EtOH (4:1) mixture saturated with compound **1** as a pressure transmitting medium, because **1** dissolves in the medium at high pressure. Synchrotron X-ray diffraction was performed at room temperature under high pressure up to 4.5 GPa at NE1A of Photon Factory Advanced Ring, KEK. The measured wavelength was $\lambda = 0.4160$ Å.

Electrochemical measurement. Cyclic voltammetry was performed with an Eco Chemie AUTOLAB PGSTAT12 potentiostat in deaerated CH_2Cl_2 containing $TBAPF_6$ (0.10 M) as a supporting electrolyte at 298 K. A conventional three-electrode cell was used with a glassy carbon working electrode and a platinum wire as a counter electrode. The redox potentials were measured with respect to a reference electrode: $Ag/AgNO_3$ (1.0×10^{-2} M) with $TBAPF_6$ (0.10 M) in acetonitrile. Deaerated fresh solvents were used for measurements. The oxidation potential of ferrocene as an external standard was 0.16 V (*vs.* $Ag/AgNO_3$) in CH_2Cl_2.

Fitting of ^{1}H NMR spectra of two-site asymmetric exchange. Spectrum of two (A and B) exchanging ½-spins $S(\omega)$ is given in complex form by eqn (S1), identical to eqn (2) in the main manuscript;

$$
\begin{aligned}
S(\omega) &= \frac{M_\mathrm{A}^0 k_\mathrm{A} + M_\mathrm{B}^0 k_\mathrm{B} + M_\mathrm{A}^0 \alpha_\mathrm{B} + M_\mathrm{B}^0 \alpha_\mathrm{A}}{\alpha_\mathrm{A}\alpha_\mathrm{B} - k_\mathrm{A} k_\mathrm{B}} \\
\alpha_\mathrm{A} &= R_{2\mathrm{A}} + k_\mathrm{A} - i(\omega - \omega_\mathrm{A}) \\
\alpha_\mathrm{B} &= R_{2\mathrm{B}} + k_\mathrm{B} - i(\omega - \omega_\mathrm{B}) \\
K_\mathrm{r} &= \frac{M_\mathrm{B}^0}{M_\mathrm{A}^0} = \frac{p_\mathrm{B}}{p_\mathrm{A}} = \frac{k_\mathrm{A}}{k_\mathrm{B}}
\end{aligned}
\tag{S1}
$$

where M_A^0 and M_B^0 are equilibrium magnetizations of A and B state, respectively. Relative populations of these states are $p_\mathrm{A} = M_\mathrm{A}^0/(M_\mathrm{A}^0 + M_\mathrm{B}^0)$, $p_\mathrm{B} = M_\mathrm{B}^0/(M_\mathrm{A}^0 + M_\mathrm{B}^0)$ and $p_\mathrm{A} + p_\mathrm{B} = 1$. $R_{2\mathrm{A}}$ and $R_{2\mathrm{B}}$ (s^{-1}) are spin-spin relaxation rates of each state, ω_A and ω_B (rad s^{-1}) are resonance frequencies of each state when no exchange is present ($k_\mathrm{A} = k_\mathrm{B} = 0$ s^{-1}), $\omega_\mathrm{A} - \omega_\mathrm{B}$ is kept constant throughout the fitting, ω (rad s^{-1}) is the angular frequency (an independent variable), i is the unit imaginary number and K_r is (temperature dependent) equilibrium constant of reaction. Experimentally, the real part $\mathrm{Re}\{S(\omega)\}$, which corresponds to absorption spectrum, of eqn (S1) is observed. After some algebraic manipulations the real part has the form of eqn (S2), which is fitted to experimentally recorded spectra.

$$\mathrm{Re}\{S(\omega)\} = \frac{(M_\mathrm{A}^0 B + M_\mathrm{B}^0 A)C + (M_\mathrm{A}^0(\omega - \omega_\mathrm{B}) + M_\mathrm{B}^0(\omega - \omega_\mathrm{A}))D}{C^2 + D^2}$$

$$A = R_{2\mathrm{A}} + k_\mathrm{A} + k_\mathrm{B}$$

$$B = R_{2\mathrm{B}} + k_\mathrm{A} + k_\mathrm{B}$$

$$C = (R_{2\mathrm{A}} + k_\mathrm{A})(R_{2\mathrm{B}} + k_\mathrm{B}) - k_\mathrm{A} k_\mathrm{B} - (\omega - \omega_\mathrm{A})(\omega - \omega_\mathrm{B})$$

$$D = (R_{2\mathrm{A}} + k_\mathrm{A})(\omega - \omega_\mathrm{B}) + (R_{2\mathrm{B}} + k_\mathrm{B})(\omega - \omega_\mathrm{A})$$

$$k_\mathrm{B} = k_\mathrm{A} \frac{M_\mathrm{A}^0}{M_\mathrm{B}^0} \tag{S2}$$

During the fitting procedure using eqn (S2) the ω, ω_A and ω_B values (rad s^{-1}) are converted to δ, δ_A and δ_B values (ppm) using the relation $\omega = 2\pi v_0 \delta$, where v_0 is the operating frequency of the spectrometer (MHz); in the present case 399.78 MHz. The difference between ω_A and ω_B is kept constant during the fitting process. Linear function was used as a baseline. After fitting spectra at low temperatures (25–50 °C) initial values of $R_{2\mathrm{A}}$, $R_{2\mathrm{B}}$ and $\omega_\mathrm{A} - \omega_\mathrm{B}$ are determined and kept constant during subsequent fitting. From fitting of remaining spectra these independent parameters are obtained: M_A^0, M_B^0, k_A and ω_A (i.e. δ_A).

Linear plots of Eyring and van't Hoff equations. Eyring equation for mean exchange rate k (s^{-1}) of unimolecular reaction in solution is:

$$k = \frac{k_\mathrm{Boltz} T}{h} e^{-\frac{\Delta G_0^\ddagger}{RT}} \tag{S3}$$

where

$$\Delta G_0^{\ddagger} = E_{\mathrm{exp}} - RT - T\Delta S_0^{\ddagger}$$

(S4)

where e is Euler number, k_{Boltz} is Boltzmann constant, h is Planck constant, R is gas constant and T is absolute temperature. $\Delta G_0^{\ddagger}$ is standard Gibbs energy change of activation to transition state (TS‡). E_{exp} is experimental activation energy (per mole) and $\Delta S_0^{\ddagger}$ is standard entropy changes of activation. Substitution of eqn (S4) into eqn (S3) and linearization yields following formula;

$$\ln\frac{k}{T} = \ln\frac{e\,k_{\mathrm{Boltz}}}{h} + \frac{\Delta S_0^{\ddagger}}{R} - \frac{1}{T}\frac{E_{\mathrm{exp}}}{R}$$

(S5)

where slope $p = -E_{\mathrm{exp}}/R$ and intercept $q = \ln(e\,k_{\mathrm{Boltz}}/h) + \Delta S_0^{\ddagger}/\mathrm{R}$. Plot of $\ln(k/T)$ *vs.* $1/T$ gives p and q. Values of E_{exp} and $\Delta S_0^{\ddagger}$ are then given by:

$$E_{\mathrm{exp}} = -Rp$$

(S6)

$$\Delta S_0^{\ddagger} = R\left(q - \ln\frac{e\,k_{\mathrm{Boltz}}}{h}\right)$$

(S7)

van’t Hoff equation for equilibrium constant of reaction K_{r} has following form:

$$K_{\mathrm{r}} = e^{-\frac{\Delta G_{0\mathrm{r}}}{RT}}$$

(S8)

where

$$\Delta G_{0\mathrm{r}} = \Delta H_{0\mathrm{r}} - T\Delta S_{0\mathrm{r}}$$

(S9)

where $\Delta G_{0\mathrm{r}}$ is standard Gibbs energy change of reaction. $\Delta H_{0\mathrm{r}}$ and $\Delta S_{0\mathrm{r}}$ are standard enthalpy and entropy change of reaction, respectively. Substitution of eqn (S9) into eqn (S8) and linearization yields following formula:

$$-R\ln K_{\mathrm{r}} = -\Delta S_{0\mathrm{r}} + \frac{1}{T}\Delta H_{0\mathrm{r}}$$

(S10)

where slope $r = \Delta H_0^{\ddagger}$ and intercept $s = -\Delta S_{0\mathrm{r}}$. Plot of $-R\ln(K_{\mathrm{r}})$ *vs.* $1/T$ gives r and s. Values of $\Delta H_{0\mathrm{r}}$ and $\Delta S_{0\mathrm{r}}$ are then given by:

$$\Delta H_{0\mathrm{r}} = r$$

(S11)

$$\Delta S_{0\mathrm{r}} = -s$$

(S12)

Materials. Reagents and solvents were commercially supplied (Tokyo Chemical Industry, Sigma-Aldrich, Wako Pure Chemical Industries and Kanto Chemical) and used as received unless otherwise noted. Ferrocene and tetrabutylammonium hexafluorophosphate (TBAPF$_6$) were purified according to the literature.[7] The synthetic methods and characterization data for 9,9'-BF derivatives (**1** and **2**) are shown below. Pristine 9,9'-BF (**3**) is commercially available from Wako Pure Chemical Industries, and also obtained as a side product during the synthesis of **2**. The NMR spectra (in CDCl$_3$ at 25 °C) of **1** and **2** are shown in Fig. S1 and S2.

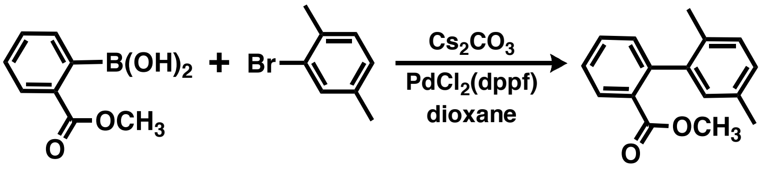

Under argon, a mixture of 2-(methoxycarbonyl)phenylboronic acid (729 mg, 4.05 mmol), 2-bromo-*p*-xylene (500 mg, 2.70 mmol), dichloro[1,1'-bis(diphenylphosphino)-ferrocene] palladium (PdCl$_2$(dppf); 99 mg, 0.14 mmol) and cesium carbonate (Cs$_2$CO$_3$; 1320 mg, 4.05 mmol) in anhydrous dioxane (11 mL) was stirred at 95 °C for 16 h. Upon cooling to r.t., the mixture was extracted with CH$_2$Cl$_2$ and the organic layer was dried over Na$_2$SO$_4$. Rotary evaporation gave a brown oil, which was purified by silica gel column chromatography (CH$_2$Cl$_2$) to yield the yellow oil product (379 mg, 58%). ^{1}H NMR (400 MHz, CDCl$_3$): δ (ppm) = 2.02 (s, 3H), 2.33 (s, 3H), 3.63 (s, 3H), 6.90 (s, 1H), 7.09 (m, 2H), 7.23 (d, J = 7.8

Hz, 1H), 7.41 (t, *J* = 7.8 Hz, 1H), 7.53 (t, *J* = 7.8 Hz, 1H), 7.94 (d, *J* = 7.8 Hz, 1H). ^{13}C NMR (101 MHz, $CDCl_3$): δ (ppm) = 19.61, 21.08, 52.00, 127.14, 128.09, 129.30, 129.43, 130.00, 130.51, 131.11, 131.64, 132.31, 134.67, 141.38, 143.21, 168.02.

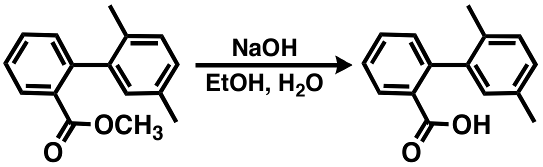

To a solution of the resultant ester (377 mg, 1.57 mmol) was added 4 mL of a NaOH aqueous solution (2.61 M) in 6 mL EtOH, and the mixture was refluxed for 3 h. The reaction mixture was cooled to r.t., followed by adding conc. HCl until the pH value of the solution was 3–4. The mixture was extracted with CH_2Cl_2 and the organic layer was dried over Na_2SO_4. Rotary evaporation afforded a yellow oil product (380 mg, quantitative). Characterization data are in accordance with published data.[8] ^{1}H NMR (400 MHz, $CDCl_3$): δ (ppm) = 2.03 (s, 3H), 2.33 (s, 3H), 6.91 (m, 1H), 7.07 (dd, *J* = 1.6 Hz, 7.8 Hz, 1H), 7.11 (d, *J* = 7.8 Hz, 1H), 7.23 (dd, *J* = 1.3 Hz, 7.6 Hz, 1H), 7.42 (td, *J* = 1.3 Hz, 7.6 Hz, 1H), 7.56 (td, *J* = 1.4 Hz, 7.5 Hz, 1H), 8.04 (m, 1H). The signal for the acid proton was not clearly observed, probably because of the fast exchange between the acid proton and H_2O (D_2O) in the $CDCl_3$ solution. ^{13}C NMR (101 MHz, $CDCl_3$): δ (ppm) = 19.64, 21.08, 127.26, 128.27, 129.19, 129.37, 129.61, 130.92, 131.46, 132.41, 132.46, 134.81, 141.03, 143.70, 171.73.

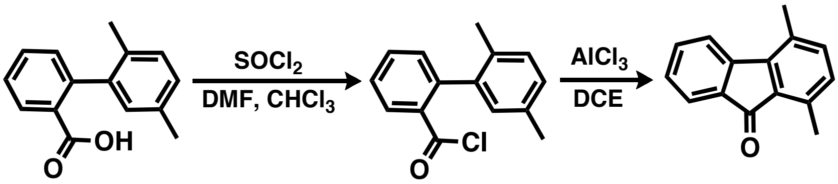

A stirred solution of the resultant carboxylic acid (370 mg, 1.63 mmol) and anhydrous dimethylformamide (DMF; 0.15 mL) in $CHCl_3$ (10 mL) was treated dropwise with $SOCl_2$ (0.44 mL, 722 mg, 6.06 mmol), and it was refluxed for 5 h. The reaction mixture was cooled and concentrated in vacuo to a brown oil, which solidified upon further standing. The low-melting solid was collected and used without further purification in the next reaction step. A mixture of the brown solid and aluminium chloride ($AlCl_3$; 586 mg, 4.41 mmol) in 1,2-dichloroethane (DCE; 5 mL) was stirred at 42 °C for 17 h, refluxed for 2 h, and then poured into cold water. The mixture was extracted with CH_2Cl_2 and the organic layer was dried over Na_2SO_4. Rotary evaporation gave an orange solid, which was purified by silica gel column chromatography (CH_2Cl_2) to yield the yellow low-melting solid product (252 mg, 74%). Characterization data are in accordance with published data.[8] ^{1}H NMR (400 MHz, $CDCl_3$): δ (ppm) = 2.56 (s, 3H), 2.60 (s, 3H), 6.95 (d, J = 7.8 Hz, 1H), 7.12 (d, J = 7.8 Hz, 1H), 7.27 (m, 1H), 7.47 (td, J = 1.2 zHz, 7.6 Hz, 1H), 7.62 (d, J = 7.6 Hz, 1H), 7.66 (ddd, J = 0.68 Hz, 1.2 Hz, 7.3 Hz, 1H). ^{13}C NMR (101 MHz, $CDCl_3$): δ (ppm) = 17.84, 20.27, 123.37, 123.98, 128.37, 131.20, 131.25, 131.81, 134.39, 134.87, 137.01, 137.13, 142.60, 144.80, 195.58.

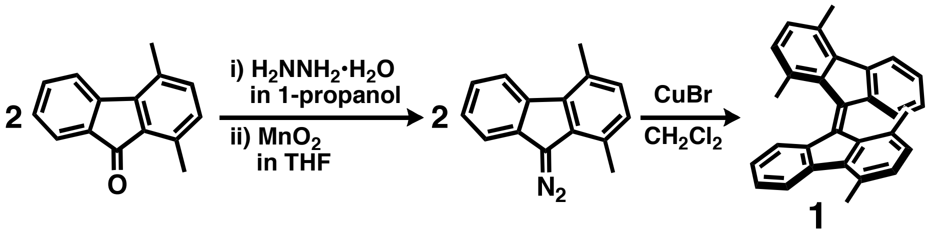

1,4-dimethyl-9-diazofluorenone was synthesized from the resultant fluorenone, according to the literature.[9] The diazo compound (120 mg, 0.55 mmol) was refluxed under Ar atmosphere for 30 min in CH_2Cl_2 (6 mL) in the presence of a catalytic amount of CuBr (2.3 mg, 0.016 mmol). Upon cooling to r.t., the reaction mixture was evaporated under reduced pressure, then the crude was purified by silica gel column chromatography (hexane:CH_2Cl_2 = 10:1) to yield a red solid. The solid was further purified by recycling preparative HPLC and recrystallization from $CHCl_3$ and MeOH to give the dark-red crystalline product (53 mg, 50%). ^{1}H NMR (400 MHz, $CDCl_3$): *trans*-state, δ (ppm) = 2.41 (s, 6H), 2.74 (s, 6H), 7.12 (m, 6H), 7.23 (m, 4H), 7.85 (d, J = 7.5 Hz, 2H). ^{13}C NMR (101 MHz, $CDCl_3$): *trans*-state, δ (ppm) = 21.09, 23.38, 123.30, 126.04, 126.48, 127.69, 130.49, 130.88, 132.22, 135.49, 137.94, 139.55, 140.34, 140.86, 141.03. Elemental analysis (calcd for $C_{30}H_{24}$: C, 93.71; H, 6.29): found C, 93.72; H, 6.25.

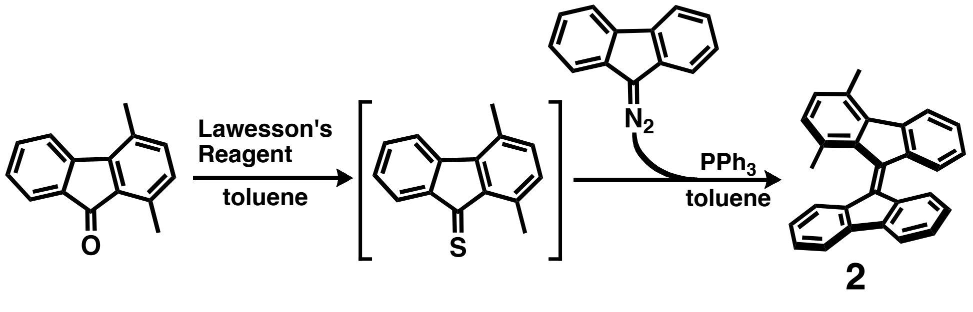

A mixture of 1,4-dimethylfluorenone (50 mg, 0.24 mmol) and Lawesson's reagent (97 mg, 0.24 mmol) in toluene anhydrous (2 mL) was refluxed under Ar atmosphere for 4 h. The formation of thioketone was checked by thin-layer chromatography and the resulting solution was used without further purification, because the thioketone is not very stable under ambient conditions. A toluene solution (4.5 mL) of 9-diazofluorenone (60 mg, 0.31 mmol) and triphenylphosphine (PPh_3; 26 mg, 0.10 mmol) was added dropwise to the resulting solution, and the mixture was refluxed under Ar atmosphere for 72 h. Upon cooling to r.t., the reaction mixture was extracted from CH_2Cl_2, and purified by silica gel column chromatography (hexane:CH_2Cl_2 = 1:1) to yield an orange-red solid. The solid containing **2** (heterodimer) and **3** (homodimer) was further purified by recycling preparative HPLC to isolate a dark-red solid of **2** (4.7 mg, 5%) and an orange-red solid of **3** (5.6 mg, 11%), respectively. The characterization data of **3** are in good accordance with those previously reported.[10] The characterization data of **2** are as follows. ^{1}H NMR (400 MHz, $CDCl_3$): δ (ppm) = 2.26 (s, 3H), 2.73 (s, 3H), 7.05 (d, J = 7.8 Hz, 1H), 7.14 (m, 3H), 7.20 (m, 1H), 7.28 (td, J = 7.4 Hz and 1.1 Hz, 3H), 7.36 (td, J = 7.4 Hz and 1.1 Hz, 1H), 7.70 (dt, J = 7.5 Hz and 0.8 Hz, 1H), 7.73 (m, 1H), 7.86 (d, J = 7.6 Hz, 1H), 8.34 (d, J = 7.7 Hz, 1H), 8.52 (d, J = 7.9 Hz, 1H). ^{13}C NMR (101 MHz, $CDCl_3$): δ (ppm) = 21.16, 23.91, 119.89, 120.21, 123.50, 124.72, 126.43, 126.73, 126.89, 127.15, 127.83, 128.29, 128.70, 128.99, 130.68, 130.86, 132.58, 135.47, 137.59, 138.59, 139.82, 140.01, 140.27, 140.32, 140.70, 141.24, 141.32, 141.61. Elemental analysis (calcd for $C_{28}H_{20}$: C, 94.34; H, 5.66): found C, 94.57; H, 5.68.

2. Supporting data

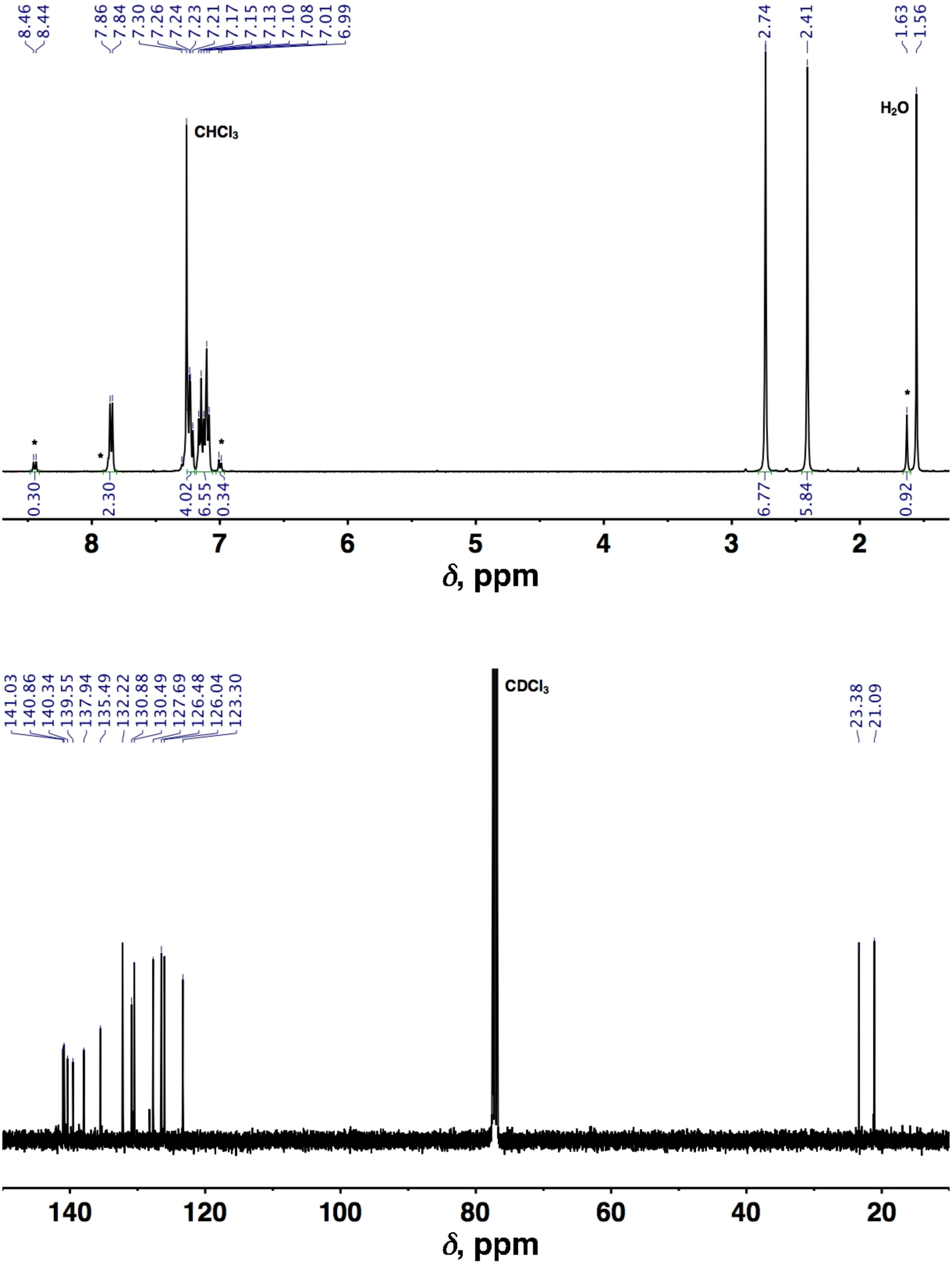

Fig. S1 ^{1}H NMR (top) and ^{13}C NMR (bottom) spectra of **1** in $CDCl_3$ at 25 °C. Major peaks are assigned to the *trans*-state, while small peaks (*) are assigned to the *cis*-state.

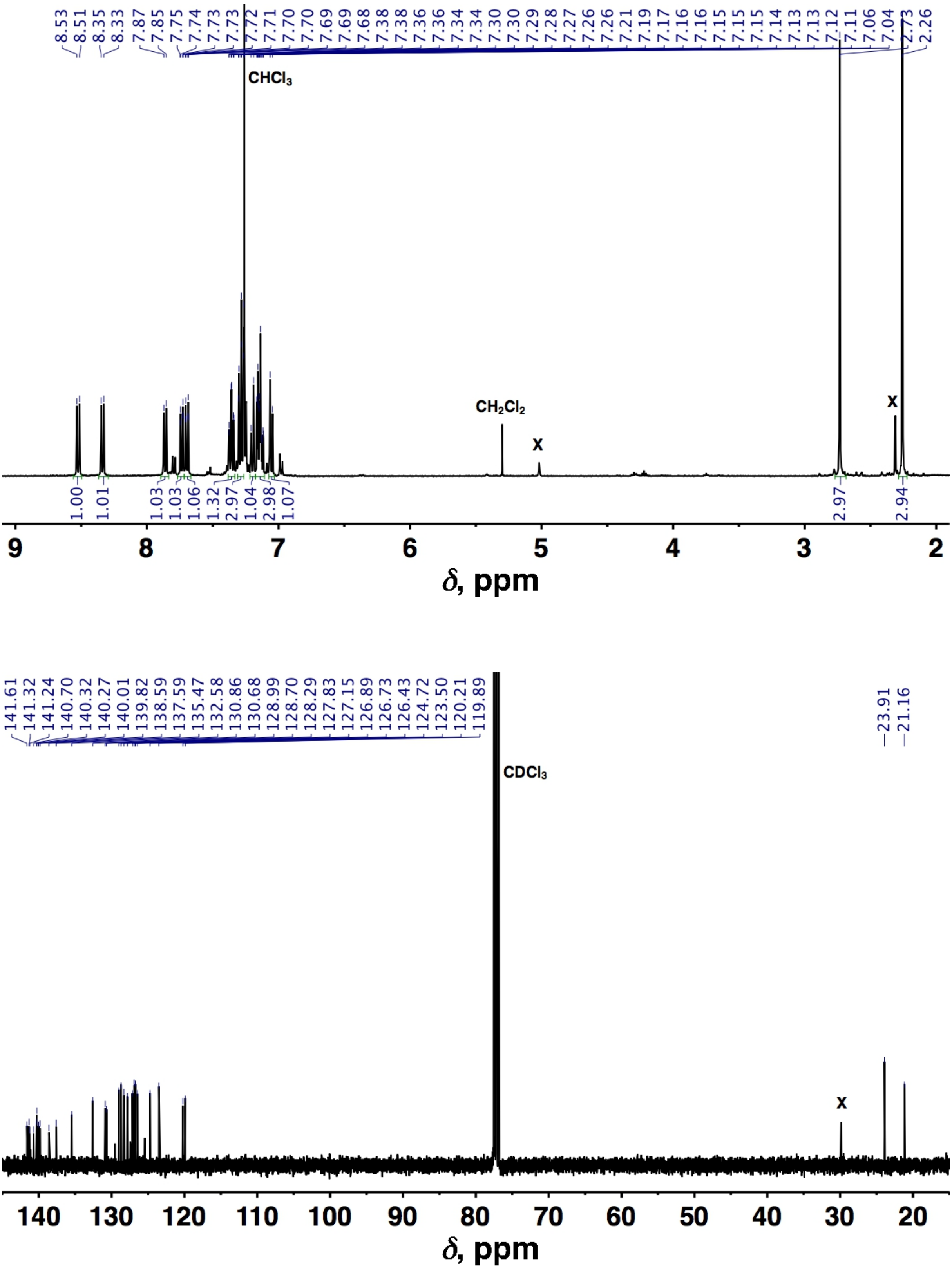

Fig. S2 ^{1}H NMR (top) and ^{13}C NMR (bottom) spectra of **2** in CDCl$_3$ at 25 °C. Small peaks (x) indicate impurities.

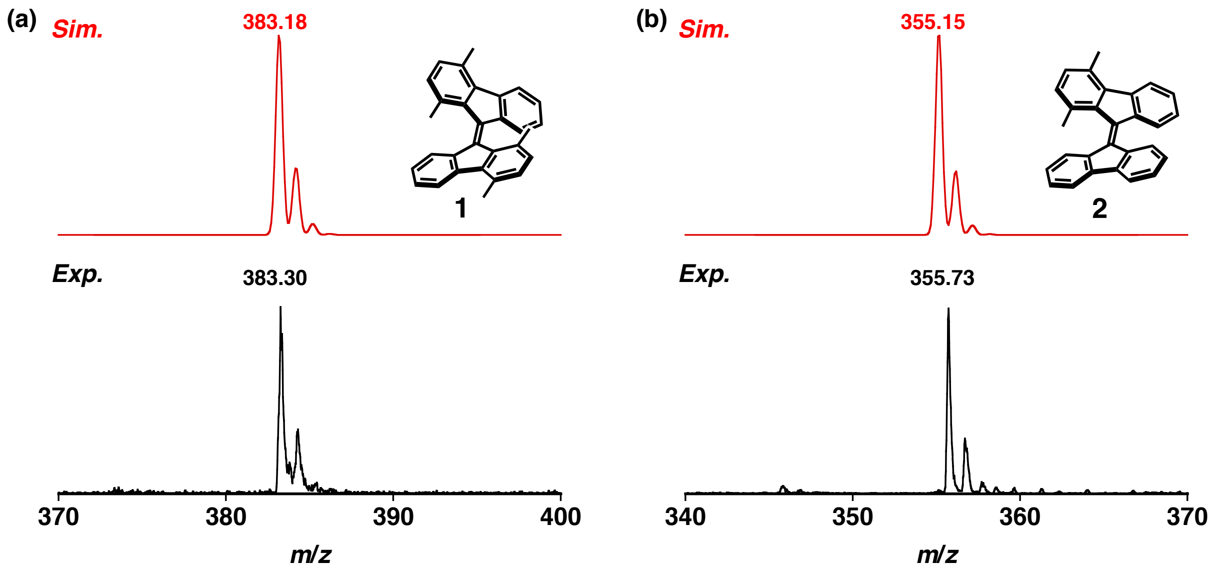

Fig. S3 MALDI/TOF-MS (positive ion, reflective mode) and the calculated isotopic distribution of (a) **1** (calcd for $C_{30}H_{24}$; $[M–1]^+$) and (b) **2** (calcd for $C_{28}H_{20}$; $[M–1]^+$).

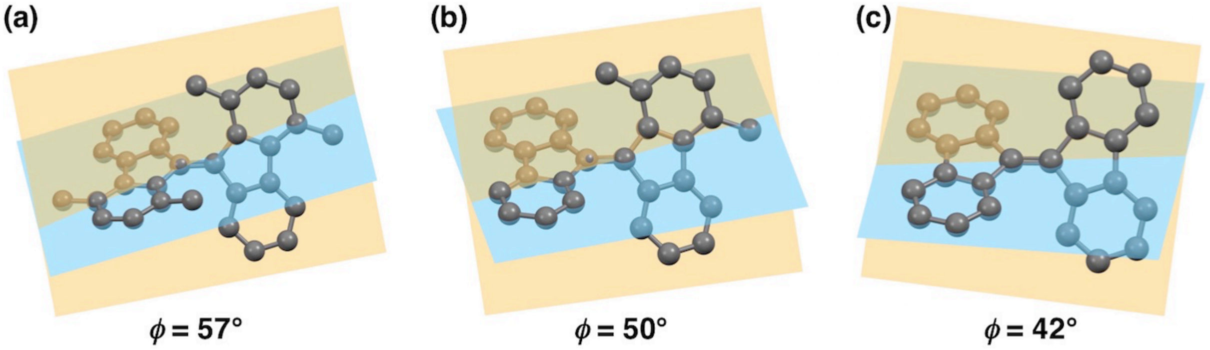

Fig. S4 Optimized structure and dihedral angle of the two fluorene π-planes of (a) **1**, (b) **2** and (c) **3** calculated by DFT at the B3LYP/6-31G(d,p) level. The dihedral angle (ϕ) between the two fluorene π-planes in each optimized geometry is also shown.

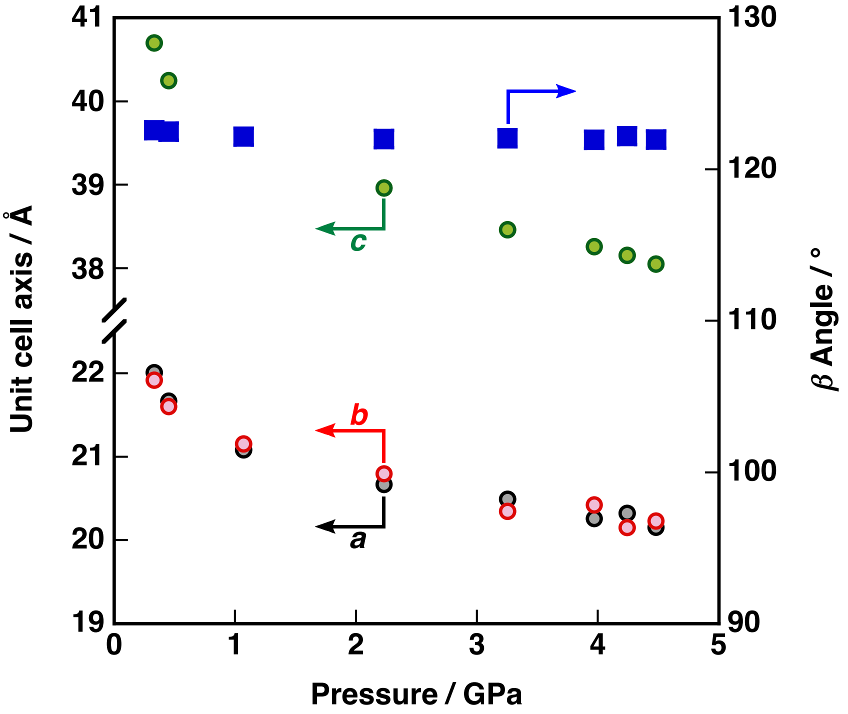

Fig. S5 Experimental pressure dependence of the normalized unit cell axes and β angle upon hydrostatic compression of **1**. Note that the angle parameters (α and γ) kept constant at 90° in the measurement pressure range.

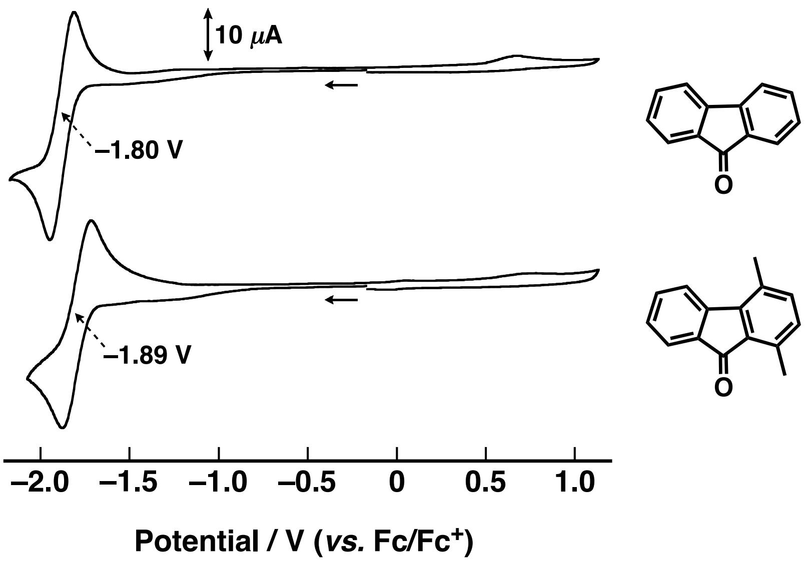

Fig. S6 Cyclic voltammogram (scan rate: 100 mV s^{-1}) of fluorenone (top) and 1,4-dimethylfluorenone (bottom) in deaerated CH_2Cl_2 (5.0×10^{-4} M) containing 0.1 M $TBAPF_6$.

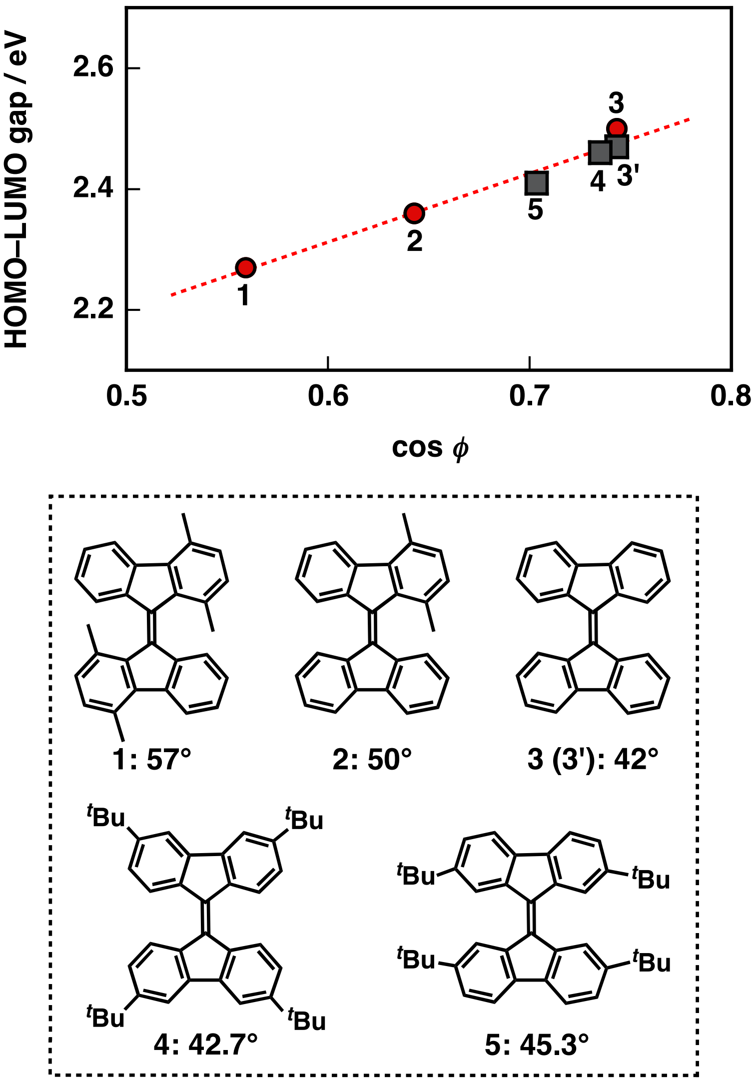

Fig. S7 Plot of HOMO–LUMO gap (E_{ox}–E_{red} / eV) obtained from cyclic voltammetry versus cos ϕ of 9,9'-BF derivatives. Red circles correspond to **1**, **2** and **3**, while gray squares (**3'**, **4** and **5**) correspond to the extracted data from a literature of 9,9'-BF, 3,6,3',6'-tetra-*tert*-Bu-9,9'-BF and 2,7,2',7'-tetra-*tert*-Bu-9,9'-BF, respectively.[11]

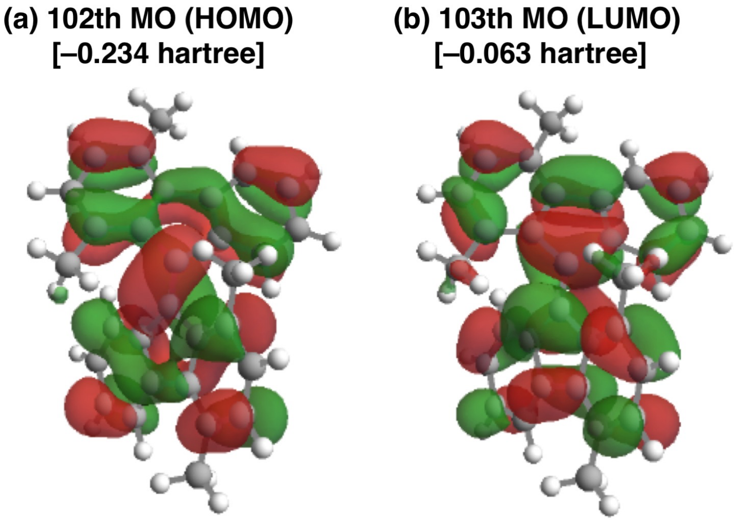

(a) 102th MO (HOMO) [–0.234 hartree]

(b) 103th MO (LUMO) [–0.063 hartree]

Fig. S8 (a) HOMO and (b) LUMO of **1** at the S_0-state geometry optimized using the DFT(M06-2X) method.

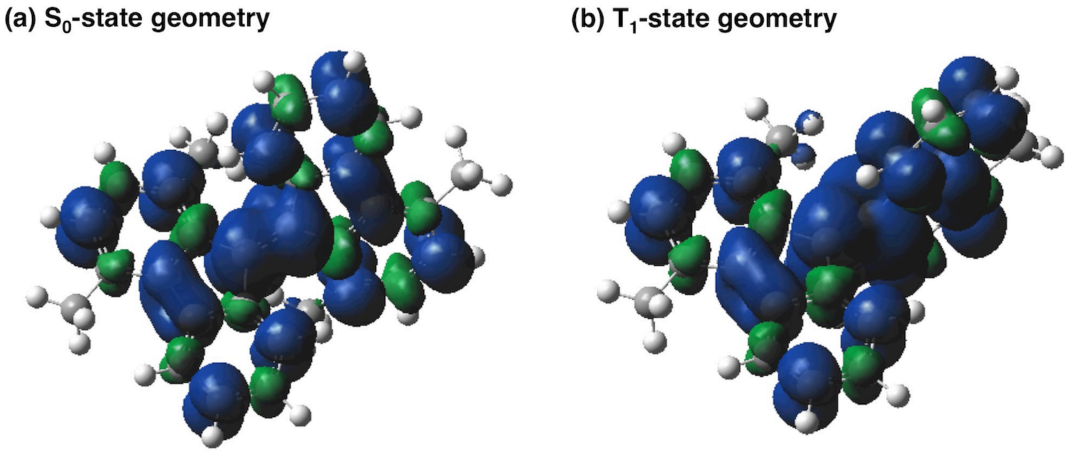

Fig. S9 The spin density distribution in the T_1 state of **1** at the (a) S_0- and (b) T_1-state geometries.

Table S1 X-ray crystallographic data for **1** at 1 atm

Formula	$C_{30}H_{24}$
Formula weight	384.49
Crystal system	monoclinic
Space group	*Cc*
T / K	213(2)
a / Å	21.7066(8)
b / Å	21.7067(8)
c / Å	20.1949(13)
β / deg.	122.509(3)
V / Å^3	8024.4(7)
Z	16
No. of reflections measured	25013
No. of observations	12072
No. of parameters refined	1098
$R1$	0.0776
$wR2$	0.1578 ($I > 2.0\sigma(I)$)
GOF	0.874
CCDC no.	1531665

Table S2 Synchrotron X-ray crystallographic data for **1** under variable hydrostatic pressure

Pressure / GPa	a / Å	b / Å	c / Å ^{a}	β / deg.
0.3	22.008(12)	21.920(11)	40.701(22)	122.602(8)
0.5	21.668(11)	21.604(10)	40.250(20)	122.500(7)
1.1	21.085(2)	21.157(17)	39.597(3)	122.183(5)
2.2	20.671(9)	20.799(10)	38.963(16)	122.005(2)
3.3	20.495(11)	20.349(9)	38.463(17)	122.061(7)
4.0	20.262(9)	20.425(11)	38.260(16)	121.958(2)
4.2	20.327(17)	20.154(13)	38.157(25)	122.197(11)
4.5	20.157(9)	20.234(51)	38.055(11)	121.979(21)

[a] The c axis determined in this experimental setup (0–4.5 GPa) is double that obtained from the single crystal X-ray structural analysis at 1 atm.

Table S3 Data (at selected temperatures) obtained from NMR spectral fitting of A ($\mathbf{1}_{trans}$) and B ($\mathbf{1}_{cis}$) exchange

Temperature / °C	k_A / s^{-1}	k_B / s^{-1}	K_r	p_A	p_B
150	3338	12008	0.278	0.782[a]	0.218[a]
140	2011	7418	0.271	0.787[a]	0.213[a]
130	1077	4080	0.264	0.791[a]	0.209[a]
110	294	1174	0.250	0.800	0.200
100	144	581	0.247	0.802	0.198
90	71	296	0.239	0.807	0.193
75	20	94	0.213	0.824	0.176
50	2.7	14	0.203	0.832	0.168
35	< 1	2.7	0.189	0.841	0.159
25	< 1	< 1	0.182	0.846	0.154

[a] Extrapolated values where K_r is not possible to retrieve from fits.

Table S4 Energy levels of **1** in the singlet and triplet states at the S_0-state optimized geometry

Solution	Spin State	ΔE / eV	λ / nm	Oscillator strength	Configuration			
					Occupied and unoccupied MO			Coeff.
1	T	1.607	771.6	0.000	102	→	103	0.690
					102	←	103	0.113
2	T	2.778	446.2	0.000	101	→	103	0.655
					100	→	104	–0.148
					98	→	103	0.126
3	T	2.796	443.5	0.000	100	→	103	0.644
					99	→	103	0.168
					101	→	104	–0.149
4	S	2.865	432.8	0.467	102	→	103	0.702
5	S	3.180	389.9	0.001	101	→	103	0.692
6	S	3.208	386.4	0.012	100	→	103	0.683
					99	→	103	0.142
7	T	3.575	346.8	0.000	99	→	103	0.635
					100	→	103	–0.189
					102	→	106	–0.147
					98	→	108	–0.105
8	T	3.678	337.1	0.000	98	→	103	0.636
					102	→	107	–0.167
					101	→	103	–0.150
					99	→	108	–0.110
9	T	4.008	309.4	0.000	100	→	105	0.405
					101	→	104	0.405
					102	→	105	0.249
					100	→	103	0.153
					98	→	104	–0.115
10	T	4.012	309.1	0.000	101	→	105	0.424
					100	→	104	0.406
					102	→	104	0.221
					101	→	103	0.156
					98	→	105	–0.114

Table S5 Energy levels of **1** in the singlet and triplet states at the T_1-state optimized geometry

Solution	Spin State	ΔE / eV	λ / nm	Oscillator strength	Configuration			
					Occupied and unoccupied MO			Coeff.
1	T	–0.333	–3724.2	0.000	102B	→	103B	–0.844
					102A	→	103A	0.844
					102B	←	103B	0.476
					102A	←	103A	–0.476
2	S	0.414	2998.3	0.023	102B	→	103B	0.900
					102A	→	103A	0.900
					102B	←	103B	–0.570
					102A	←	103A	–0.570
					94B	→	103B	0.107
					94A	→	103A	0.107
3	T	1.721	720.6	0.000	101B	→	103B	–0.688
					101A	→	103A	0.688
					98B	→	103B	–0.124
					98A	→	103A	0.124
4	T	1.803	687.8	0.000	100B	→	103B	–0.680
					100A	→	103A	0.680
					99B	→	103B	–0.159
					99A	→	103A	0.159
5	S	1.962	631.9	0.001	101B	→	103B	0.698
					101A	→	103A	0.698
6	S	2.038	608.4	0.000	100B	→	103B	0.692
					100A	→	103A	0.692
					99B	→	103B	0.126
					99A	→	103A	0.126
7	T	2.550	486.2	0.000	99B	→	103B	–0.674
					99A	→	103A	0.674
					100B	→	103B	0.162
					100A	→	103A	–0.162
8	T	2.671	464.1	0.000	98B	→	103B	–0.675
					98A	→	103A	0.675
					101B	→	103B	0.128
					101A	→	103A	–0.128
					102B	→	106B	0.117
					102A	→	106A	–0.117
9	S	3.020	410.6	0.084	99B	→	103B	0.682
					99A	→	103A	0.682
					100B	→	103B	–0.128
					100A	→	103A	–0.128
10	S	3.144	394.4	0.091	98B	→	103B	0.685
					98A	→	103A	0.685

Table S6 Energy levels of **3** in the singlet and triplet states at the S_0-state optimized geometry

Solution	Spin State	ΔE / eV	λ / nm	Oscillator strength	Configuration			
					Occupied and unoccupied MO			Coeff.
1	T	1.727	717.9	0.000	86	→	87	0.692
					86	←	87	0.106
2	T	2.836	437.2	0.000	84	→	87	0.659
					85	→	89	0.128
					82	→	87	0.117
					85	→	92	0.104
3	T	2.850	435.0	0.000	85	→	87	0.654
					83	→	87	0.136
					84	→	89	0.128
					84	→	92	0.107
4	S	2.999	413.4	0.503	86	→	87	0.703
5	S	3.248	381.7	0.001	84	→	87	0.696
6	S	3.254	381.0	0.000	85	→	87	0.696
7	T	3.811	325.3	0.000	83	→	87	0.565
					86	→	90	–0.222
					85	→	87	–0.202
					85	→	88	0.141
					82	→	92	0.129
					81	→	91	0.125
					84	→	89	0.122
8	T	3.895	318.3	0.000	82	→	87	0.504
					84	→	88	0.232
					85	→	89	0.213
					84	→	87	–0.201
					86	→	91	0.193
					81	→	90	–0.146
					83	→	92	0.132
					82	→	88	–0.102
9	T	4.001	309.9	0.000	85	→	88	0.457
					84	→	89	0.419
					83	→	87	–0.262
10	T	4.013	309.0	0.000	84	→	88	0.413
					85	→	89	0.388
					82	→	87	−0.376

Table S7 Energy levels of **3** in the singlet and triplet states at the T_1-state optimized geometry

Solution	Spin State	ΔE / eV	λ / nm	Oscillator strength	Configuration			
					Occupied and unoccupied MO			Coeff.
1	T	–0.572	–2166.1	0.000	86B	→	87B	–0.717
					86A	→	87A	0.717
					86B	←	87B	–0.182
					86A	←	87A	0.182
2	S	1.644	754.4	0.269	86B	→	87B	0.723
					86A	→	87A	0.723
					86B	←	87B	–0.185
					86A	←	87A	–0.185
3	T	2.127	582.9	0.000	85B	→	87B	0.683
					85A	→	87A	–0.683
					83B	→	87B	0.119
					83A	→	87A	–0.119
4	T	2.173	570.6	0.000	84B	→	87B	0.686
					84A	→	87A	–0.686
					82B	→	87B	–0.105
					82A	→	87A	0.105
5	S	2.419	512.6	0.001	85B	→	87B	0.700
					85A	→	87A	0.700
6	S	2.457	504.7	0.001	84B	→	87B	0.700
					84A	→	87A	0.700
7	T	3.184	389.4	0.000	83B	→	87B	0.663
					83A	→	87A	–0.663
					86B	→	90B	–0.156
					86A	→	90A	0.156
					85B	→	87B	–0.133
					85A	→	87A	0.133
8	T	3.314	374.1	0.000	82B	→	87B	0.664
					82A	→	87A	–0.664
					86B	→	91B	–0.155
					86A	→	91A	0.155
					84B	→	87B	0.120
					84A	→	87A	–0.120
9	T	3.555	348.8	0.000	86B	→	88B	0.680
					86A	→	88A	–0.680
10	S	3.644	340.2	0.047	83B	→	87B	0.682
					83A	→	87A	0.682
					85B	→	88B	0.107
					85A	→	88A	0.107

3. References

1 G. R. Fulmer, A. J. M. Miller, N. H. Sherden, H. E. Gottlieb, A. Nudelman, B. M. Stoltz, J. E. Bercaw and K. I. Goldberg, *Organometallics*, 2010, **29**, 2176.

2 (*a*) M. J. Frisch, G. W. Trucks, H. B. Schlegel, G. E. Scuseria, M. A. Robb, J. R. Cheeseman, G. Scalmani, V. Barone, G. A. Petersson, H. Nakatsuji, X. Li, M. Caricato, A. Marenich, J. Bloino, B. G. Janesko, R. Gomperts, B. Mennucci, H. P. Hratchian, J. V. Ortiz, A. F. Izmaylov, J. L. Sonnenberg, D. Williams-Young, F. Ding, F. Lipparini, F. Egidi, J. Goings, B. Peng, A. Petrone, T. Henderson, D. Ranasinghe, V. G. Zakrzewski, J. Gao, N. Rega, G. Zheng, W. Liang, M. Hada, M. Ehara, K. Toyota, R. Fukuda, J. Hasegawa, M. Ishida, T. Nakajima, Y. Honda, O. Kitao, H. Nakai, T. Vreven, K. Throssell, J. A. Montgomery, Jr., J. E. Peralta, F. Ogliaro, M. Bearpark, J. J. Heyd, E. Brothers, K. N. Kudin, V. N. Staroverov, T. Keith, R. Kobayashi, J. Normand, K. Raghavachari, A. Rendell, J. C. Burant, S. S. Iyengar, J. Tomasi, M. Cossi, J. M. Millam, M. Klene, C. Adamo, R. Cammi, J. W. Ochterski, R. L. Martin, K. Morokuma, O. Farkas, J. B. Foresman and D. J. Fox, *Gaussian 09, Revision D.01*, Gaussian, Inc., Wallingford, Connecticut, 2016; (*b*) R. Dennington, T. Keith and J. Millam, *GaussView, Version 5*, Semichem Inc., Shawnee Mission, Kansas, 2009.

3 *CrystalClear*, Rigaku Corporation, Akishima, Tokyo, 2005.

4 G. M. Sheldrick, *Acta Crystallogr., Sect. A: Found. Adv.*, 2015, **71**, 3.

5 G. M. Sheldrick, *Acta Crystallogr., Sect. C: Struct. Chem.*, 2015, **71**, 3.

6 L. J. Farrugia, *J. Appl. Crystallogr.*, 1999, **32**, 837.

7 W. L. F. Armarego and C. L. L. Chai, *Purification of Laboratory Chemicals, 6th ed.*, Elsevier Inc., Oxford, 6th edn., 2009.

8 S. R. D. George, T. E. Elton and J. B. Harper, *Org. Biomol. Chem.*, 2015, **13**, 10745.

9 J. Bauer, L. Hou, J. C. Kistemaker and B. L. Feringa, *J. Org. Chem.*, 2014, **79**, 4446.

10 S. Pogodin, S. Cohen and I. Agranat, *Eur. J. Org. Chem.*, 1999, 1979.

11 G. L. Eakins, M. W. Cooper, N. N. Gerasimchuk, T. J. Phillips, B. E. Breyfogle and C. J. Stearman, *Can. J. Chem.*, 2013, **91**, 1059.